

Effect of Cr and Mo on Corrosion Behavior of High Strength Steel in CO₂/H₂S Environments

Keiichi Kondo^{1,2}, Yoon-Seok Choi¹, Srdjan Nesic¹, Taro Ohe², Hiroki Kamitani², Hisashi Amaya², Jun Nakamura³, Yuji Arai³

¹ Institute for Corrosion and Multiphase Technology, Ohio University, 342 West State Street, Athens, OH 45701, USA

² NIPPON STEEL CORPORATION, 1850, Minato Wakayama, Wakayama 640-8555, Japan

³ NIPPON STEEL CORPORATION, 1-8, Fuso-Cho Amagasaki, Hyogo 660-0891, Japan

ABSTRACT

The effect of Cr and Mo on the corrosion behavior of high strength steel was investigated in CO₂/H₂S environments. Corrosion tests were conducted using three different types of steel; Base steel (including no Cr and no Mo), 1% Cr steel and 1% Mo steel, in 1 wt.% NaCl solution (80°C) at initial pH 5.7 and initial pH 4.2 under atmospheric pressure. The test solution was saturated with flowing CO₂/10% H₂S mixture. Changes in corrosion rate with exposure time were monitored by linear polarization resistance (LPR) measurements. The surface morphology and the composition of the corrosion product layers were analyzed by various surface analysis techniques (SEM, EDS, EPMA, and XRD). The results showed that the final corrosion rates for all three steels were low (less than 0.2 mm/y) due to the formation of protective FeS layer. However, the initial corrosion behaviors were different among the three steel types depending on the role of corrosion products including Cr and Mo.

Key words: CO₂/H₂S corrosion, high strength steel, alloying element, FeS

INTRODUCTION

The development of deep and high pressure high temperature (HPHT) oil and gas fields increase the demand for high strength steels Oil Country Tubular Goods (OCTG). In the case that the environments containing H₂S, which could occur by reservoir souring, sufficient resistance to sulfide stress cracking (SSC) is required for the high strength steel. To correspond to the trend, the high strength steels with specified minimum yield strength above 95 ksi for sour service have been developed by significant efforts.¹⁻⁹

Numerous fundamental studies have been conducted on how to improve SSC resistance mainly from the point of microstructural modification by improving the heat treatment process and chemical compositions of steel.¹⁰⁻¹⁵ To date, it has been widely recognized that the highly homogeneous tempered martensite microstructure with fine prior austenite grain produced by quenching and

tempering heat treatment process is beneficial to prevent intergranular cracking. In terms of the chemical composition of steel, it also has been generally known that the appropriate addition of Cr and Mo into steel is effective to enhance its SSC resistance by the microstructural modification.

In addition to the viewpoints of the microstructural factor, it seems to be also important to comprehend an effect of small amounts of Cr and Mo on corrosion behavior since the corrosion behavior, which includes relationship between variations of corrosion rate and formation of corrosion products with time, might affect the hydrogen behavior on steel surface and be related to the occurrence of SSC. Although there are numerous studies about the effect of Cr on the corrosion behavior of low alloy steel in CO₂ environments,¹⁶⁻²² there are not many studies about the effect of small amounts of Cr and Mo on the corrosion behavior in CO₂/H₂S environments^{17,23-25} and the effect of small amounts of Cr and Mo on the corrosion behavior has not been cleared yet, especially for high strength steels.

Thus, this present study attempted to investigate the effect of small amounts of Cr and Mo on the corrosion behavior of 125 ksi-grade high strength steel under CO₂/10%H₂S at 80°C and different initial solution pH environments. The high strength steels applied in this study were Base steel (including no Cr and no Mo), 1 % Cr steel and 1 % Mo steel, which were fabricated by laboratory scale equipment.

EXPERIMENTAL PROCEDURE

Materials

Three high strength steels with a specified minimum yield strength of 862 MPa (125 ksi) were used in the present study. The chemical compositions are shown in Table 1 as Base steel containing no Cr and Mo, 1% Cr steel, and 1% Mo steel. The steels were fabricated using a vacuum arc-melting furnace and cast into 180 kg ingots. The ingots were hot rolled into plates with 15 mm thickness, and the plates were then cooled in the air at room temperature. Subsequently, double quenching & tempering heat treatment was conducted by using a laboratory furnace. The hardness of the plates after second Quenched treatment was not less than the API 5CT criterion for 90% of martensite. The quenched steel plates were tempered at different temperatures and holding times to control the yield strength. (460°C for Base steel, 525°C for 1% Cr steel, and 650°C for 1% Mo steel). The microstructure of the three steels showed tempered martensite as shown in Figure 1.

The specimens for the corrosion test were machined with two different geometries. The specimen for electrochemical measurements had a cylindrical geometry with 1.2 cm in outer diameter and 1.4 cm in height and would have its outer surface exposed to the solution. Specimens for surface analyses were machined with rectangular shape (1.27 cm × 1.27 cm × 0.254 cm). Both types of specimens were sequentially ground with 180, 400, and then 600 grit silicon carbide (SiC) paper, cleaned with isopropyl alcohol in an ultrasonic bath and dried.

Table 1
Chemical compositions of materials used in the present study (wt.% balance Fe)

Steel type	C	Si	Mn	P	S	Cr	Mo
Base steel	0.24	0.34	0.98	0.011	0.0008	-	-
1% Cr steel	0.24	0.35	0.98	0.011	0.0008	1.01	-
1% Mo steel	0.22	0.34	1.00	0.011	0.0007	0.03	0.99

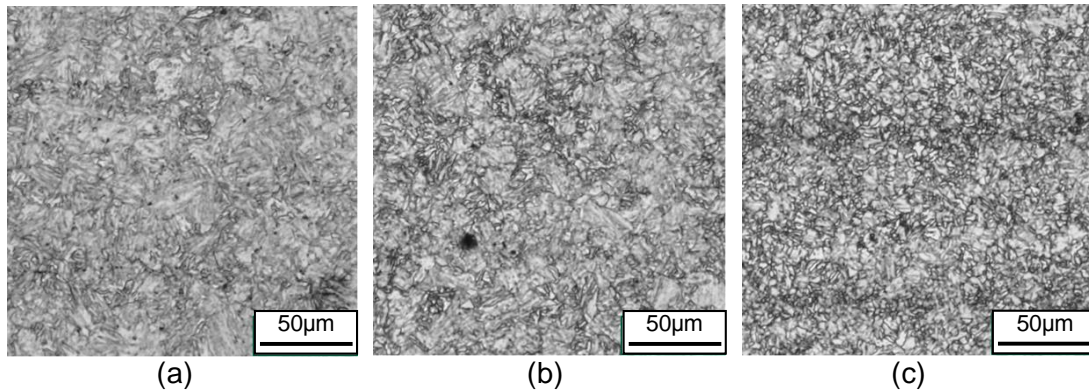


Figure 1: Optical images of the microstructure of different high strength steels (Etched by 3% nital): (a) Base steel, (b) 1%Cr steel, (c) 1%Mo steel.

Experimental Setup

Figure 2 shows the schematic of the experimental setup. Corrosion tests were carried out in a 2-L glass cell under atmospheric pressure. An aqueous electrolyte was prepared from deionized water with 1 wt.% NaCl. The setup consists of a three-electrode corrosion cell (CE: a platinum-coated titanium mesh, RE: a silver/silver chloride [Ag/AgCl] electrode), a hot plate equipped with a temperature controller, pH electrode, rotameter to adjust CO₂ and H₂S gas concentration, sparge tube as CO₂/ H₂S gas inlet, and condenser.

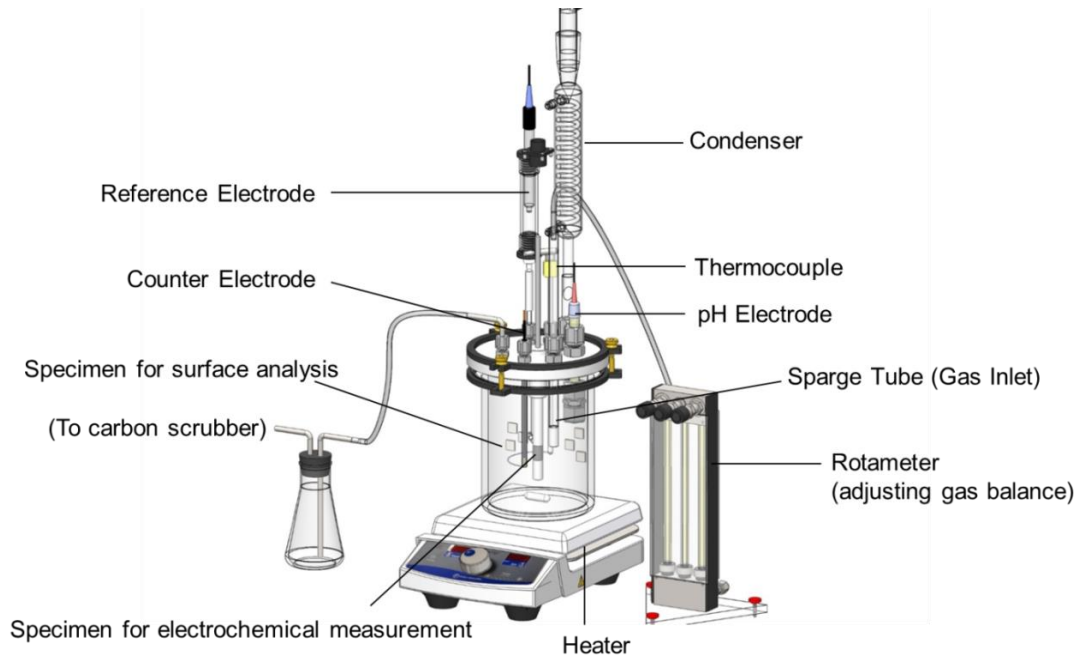


Figure 2: Schematic of the glass cell setup.

Methodology

Details of experimental conditions for the present study are shown in Table 2. At first, the solution was purged by bubbling CO₂ gas for at least 3 hours to remove oxygen. After the solution was deoxygenated, CO₂/ 10% H₂S mixed gas adjusted by the rotameter was introduced to the solution in the test cell by purging for at least 2 hours to saturate the electrolyte prior to insertion of the specimens.

The initial pH of the solution was adjusted by adding NaHCO₃ in sufficient quantity to reach the desired pH. During the corrosion experiments, the test solution was saturated with a continuous sparging of the CO₂/ 10% H₂S mixed gas.

Table 2
Detailed parameters on test conditions for corrosion testing

Parameter	Description	
Material	Base steel, 1% Cr steel, 1% Mo steel	
Partial pressure of CO ₂	CO ₂ / 10% H ₂ S (pCO ₂ = 0.48 bar, pH ₂ S = 0.053 bar)	
Temperature	80°C	
Test solution	1 wt.% NaCl	
Initial solution pH	5.7 (adjusted by NaHCO ₃)	4.2 (Natural pH)
Solution volume	2 L	
Stirring solution	Magnet stirrer 100rpm (equivalent to 0.17 m/s in a 0.1 m ID pipe) ²⁶	
Control of Fe ²⁺	Not controlled	
Control of solution pH	Not controlled	
Specimen: Electrochemical	1 cylindrical sample (0.47" dia x 0.57" length)	
Specimen: Surface analysis	4 small plates (0.5" x 0.5" x 0.1")	

The corrosion properties of high strength steels were periodically monitored by electrochemical techniques (open-circuit potential [OCP], linear polarization resistance [LPR] measurements). LPR measurements were performed within ±10 mV with respect to the corrosion potential with a scan rate of 0.166 mV/s and B value was 23 mV.²⁶ Using the polarization resistance (R_p) obtained from LPR measurement, the corrosion current density (i_{corr}) was calculated by using Eq. (1):²⁷

$$i_{\text{corr}} = \frac{B}{R_p} \quad (1)$$

Then, the i_{corr} was converted into the corrosion rate using Eq. (2):²⁸

$$\text{Corrosion rate (mm/ye ar)} = \frac{0.00327 \times i_{\text{corr}} (\mu\text{A/cm}^2) \times \text{EW}}{\text{density (g/cm}^3)} \quad (2)$$

where EW is the equivalent weight in grams and 0.00327 is a constant factor used for dimension and time conversion.

After the corrosion experiments, *ex-situ* analyses for the morphology and compositions of corrosion product layers were conducted by using scanning electron microscopy (SEM), energy dispersive x-ray spectroscopy (EDS), field emission-electron probe micro analyzer (FE-EPMA), and x-ray diffraction (XRD). The surface and cross-sectional morphologies of corrosion products were analyzed by SEM. The specimen mounted in an epoxy was used for cross-sectional analyses. The chemical analysis for the corrosion product layers was performed by using EDS, XRD, and FE-EPMA. The FE-EPMA analyses were applied for the cross-sectional specimen mounted in an epoxy.

RESULTS

Experiments at pH 5.7 and 80°C

The variations in corrosion rate and corrosion potential with time monitored by LPR measurement for the different steel types in CO₂/10% H₂S-saturated 1 wt.% NaCl at pH 5.7 and 80°C are shown in

Figure 3. Although all steels showed similar corrosion behavior with decreasing corrosion rate with time, there was a difference at the initial stage of exposure. 1% Cr steel showed an immediate decrease in the corrosion rate while 1% Mo steel took longer to reduce the corrosion rate and Base steel exhibited intermediate behavior. At the later stage of exposure, the corrosion rates of all steels eventually reached to low values (< 0.2 mm/y). In addition, the corrosion potential of all steels increased when the corrosion rate started to decrease.

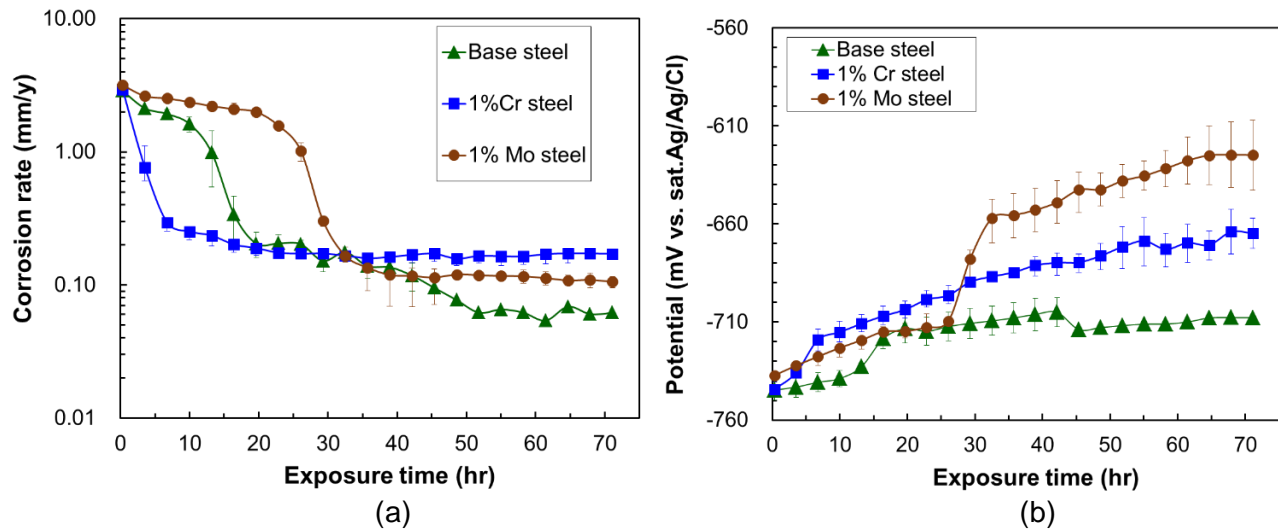
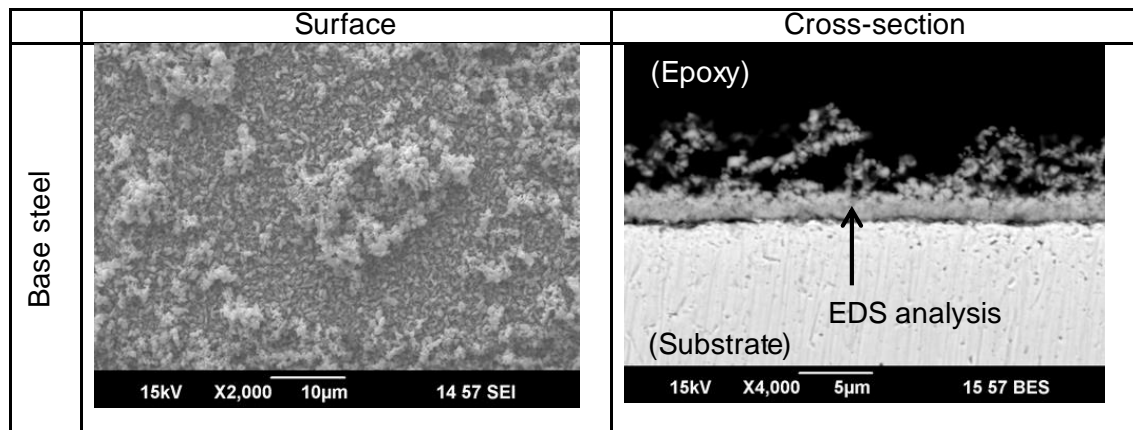


Figure 3: Variation of (a) corrosion rate and (b) corrosion potential with time obtained by LPR measurements in $\text{CO}_2/10\% \text{H}_2\text{S}$ at pH 5.7 and 80°C .

Figure 4 shows the surface and cross-sectional SEM images of the corroded samples after exposure of 20 hours. Corrosion products as small particles were observed on the top of the surface of all samples. The cross-sectional analyses revealed that the morphology of corrosion product layer was obviously different among the different type of steels. A continuous corrosion product layer was formed underneath the small particles on the surface of the Base steel and the 1% Cr steel. On the other hand, for 1% Mo steel, it is difficult to observe a continuous corrosion product layer. Compositions of the layer formed on the steel surface were analyzed by EDS as shown in Table 3. The layer formed on the surface of the Base steel includes Fe+S compound. The thin layer formed on the corroded surface of 1% Cr steel includes mainly Fe+S and small amount of Cr+O compounds. The corrosion product formed on the surface of the 1% Mo steel includes mainly Fe+S compound and likely small amount of Mo+S compound.



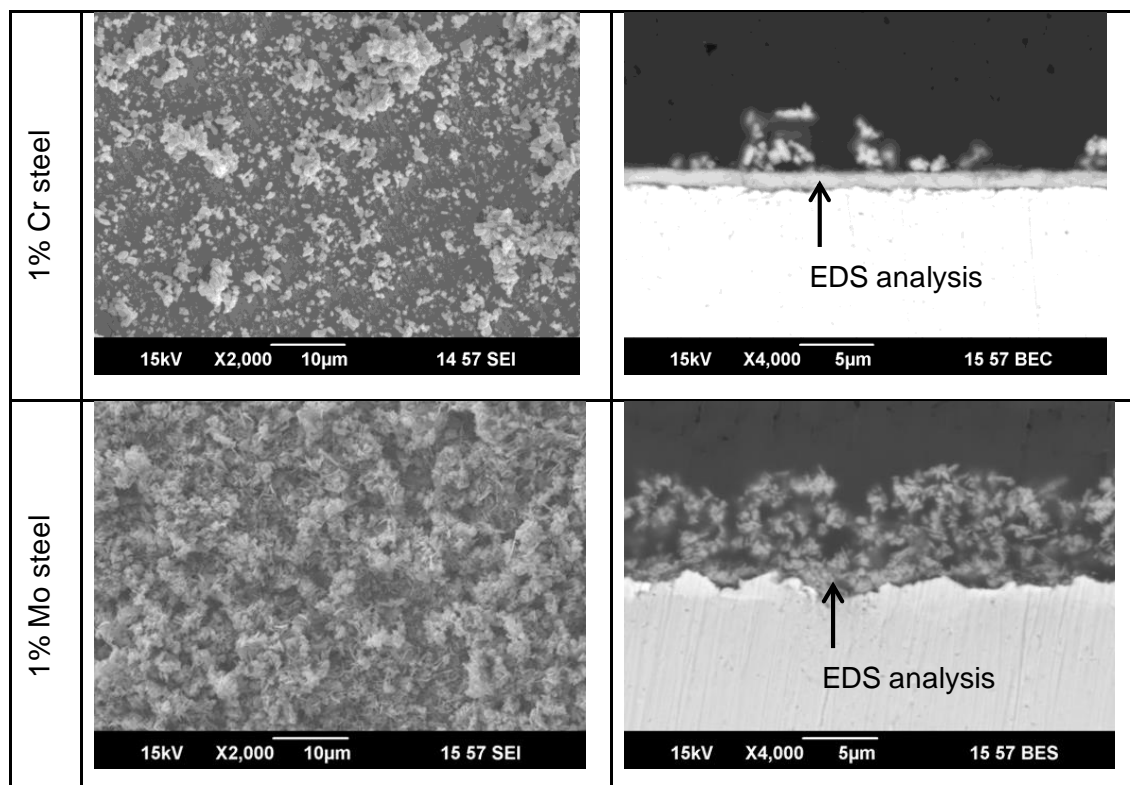


Figure 4: SEM surface and cross-section images of the corroded samples after 20 hours of exposure at pH 5.7 and 80°C.

**Table 3
Results of EDS analysis for the corrosion products formed on the sample surfaces after 20 hours of exposure**

Arrow in Figure 4	C* (at.%)	O (at.%)	S (at.%)	Fe (at.%)	Cr (at.%)	Mo (at.%)
Base steel	36.8	1.6	27.5	34.2	-	-
1% Cr steel	32.0	4.9	26.5	35.3	1.4	-
1% Mo steel	64.3	3.2	12.7	19.2	< 0.1	0.6

*C could come from epoxy

Figure 5 shows the surface and cross-sectional SEM images of the corroded samples at the end of exposure (72 hours). The surface morphology is not significantly different from the result after 20 hours. However, the cross-sectional observations show that all samples were covered by a continuous corrosion product layer with a porous outer layer.

Figure 6 shows the XRD patterns of the corroded steels after 72 hours of exposure. For all samples, FeS (mackinawite) and Fe peaks were detected by XRD. The Cr+O and Mo+S compounds were not detected by XRD because it might be an amorphous phase or too thin to be detected by XRD.

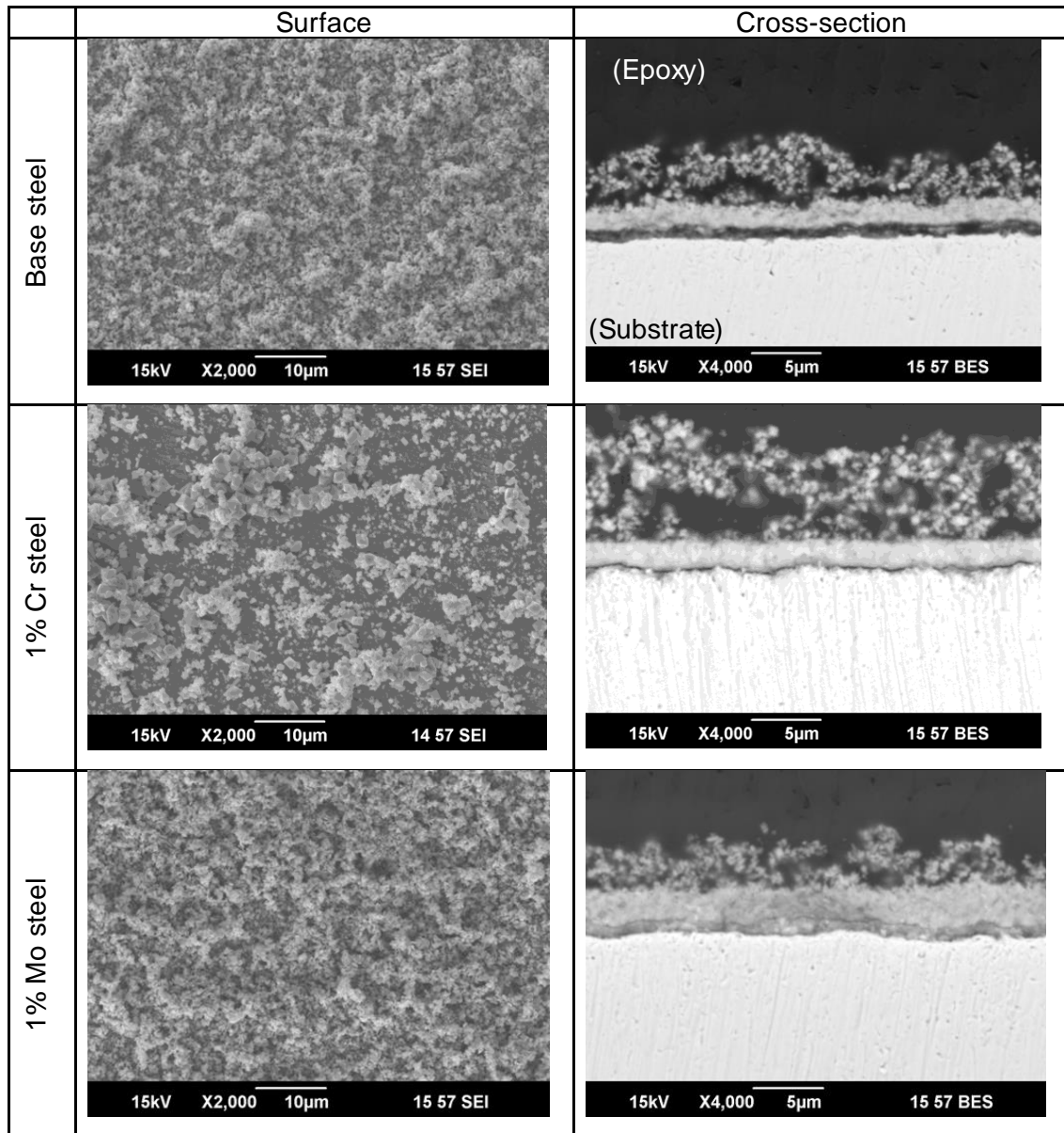


Figure 5: SEM surface and cross-section images of the corroded samples after 72 hours of exposure at pH 5.7 and 80°C.

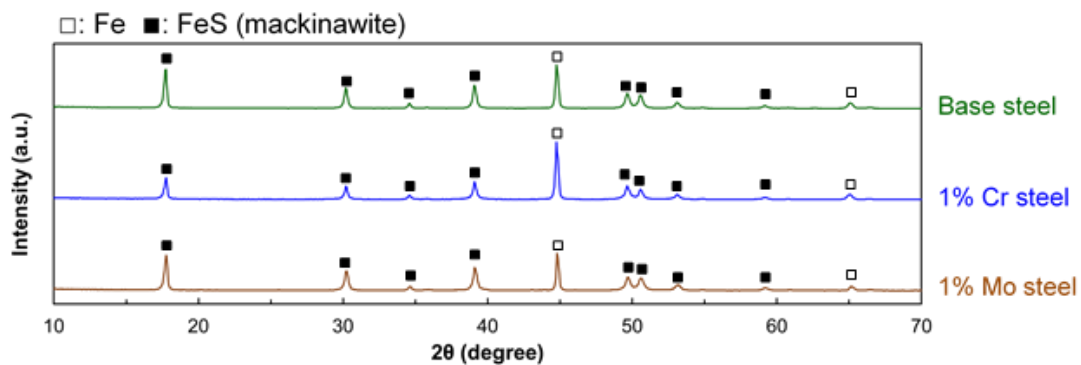


Figure 6: Results of XRD analysis for the corroded samples after 72 hours of exposure.

Experiments at pH 4.2 and 80°C

In this condition, the initial solution pH was lowered compared to the above condition. The variations in corrosion rate and corrosion potential with time monitored by LPR measurement for the different steel types in CO₂/10% H₂S-saturated 1 wt.% NaCl at pH 4.2 and 80°C are shown in Figure 7. The corrosion rate of all steels decreased with time and reached a low value (less than 0.2 mm/y). The corrosion potential of all steels increased when the corrosion rate started to decrease. When focusing on the difference of corrosion behavior at initial stage (up to around 20 hours) of exposure among different steel types, although the trend to decrease corrosion rate is similar to the corrosion behavior at initial pH 5.7 as shown in Figure 3, the difference became small.

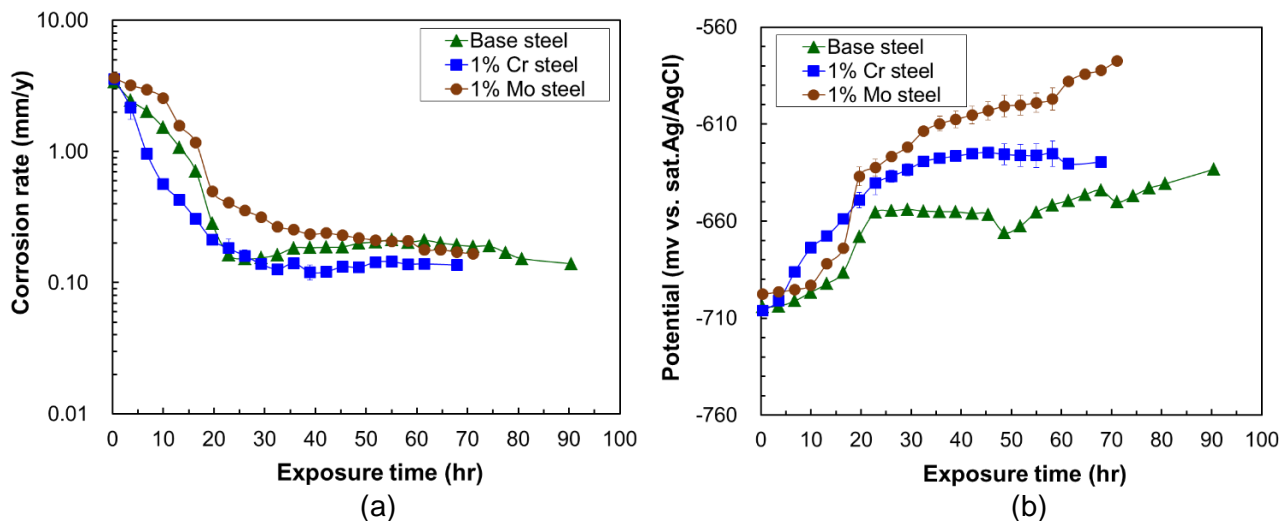
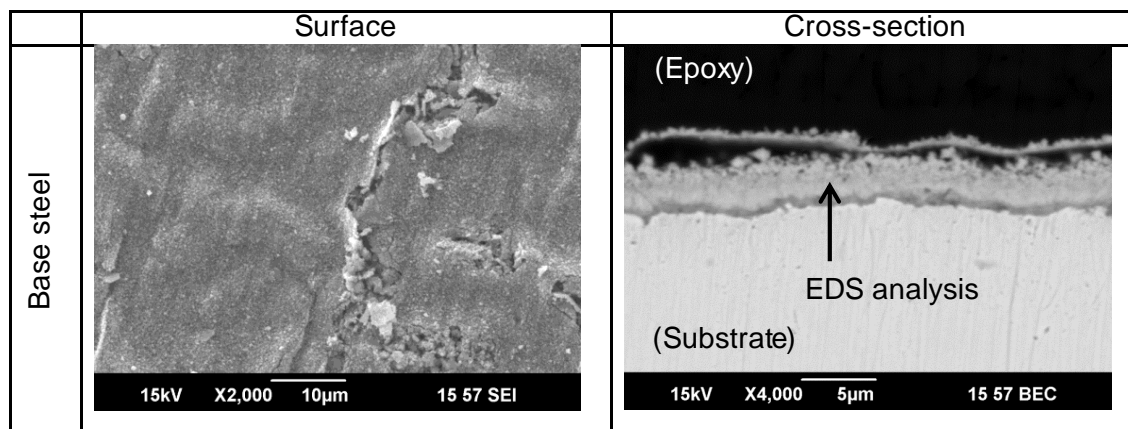


Figure 7: Variation of (a) corrosion rate and (b) corrosion potential with time obtained by LPR measurements in CO₂/10% H₂S at pH 4.2 and 80°C.

Figure 8 shows the surface and cross-sectional SEM images of the corroded samples after 20 hours of exposure. Corrosion products were observed on the top of the surface of all samples. In contrast to those in the condition at pH 5.7, the cross-sectional analyses revealed that all corroded samples showed that a continuous layer formed on the steel surface underneath a thin outer layer. Compositions of the layer formed on the corroded surface of each steel were analyzed by EDS as shown in Table 4. The layer on the Base steel could include Fe+S compound. The layer formed on the 1% Cr steel could include mainly Fe+S and small amount of Cr+O compounds. The layer formed on the 1% Mo steel could include mainly Fe+S compound and small amount of Mo+S compound.



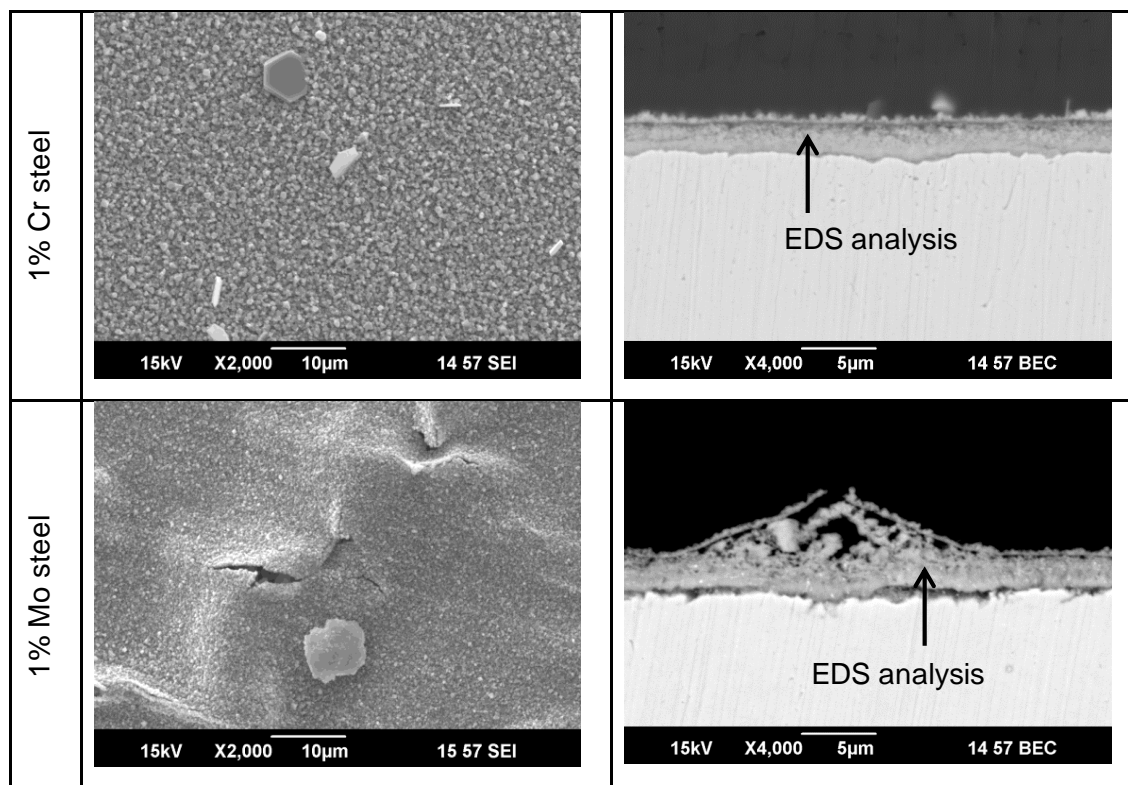


Figure 8: SEM surface and cross-section images of the corroded samples after 20 hours of exposure at pH 4.2 and 80°C.

**Table 4
Results of EDS analysis for the corrosion products formed on the sample surfaces after 20 hours of exposure**

Arrow in Figure 8	C* (at.%)	O (at.%)	S (at.%)	Fe (at.%)	Cr (at.%)	Mo (at.%)
Base steel	39.1	1.0	27.3	32.7	-	-
1% Cr steel	31.1	2.2	28.7	37.0	1.1	-
1% Mo steel	23.3	1.6	37.8	37.0	<0.1	0.3

*C could come from epoxy

Figure 9 shows the surface and cross-sectional SEM images of the corroded samples at the end of the exposure. Corrosion products were observed on the top of surface for all samples. The cross-sectional observations show that all samples were covered by the continuous corrosion product layer.

Figure 10 shows the XRD patterns of the corroded different steel types at the end of the exposure. For all samples, FeS (mackinawite) and Fe peaks were detected by XRD. The other corrosion products such as Cr+O compound in the 1% Cr steel and the Mo+S compound in the 1 % Mo steel could not be detected likely due to the same reason as mentioned above.

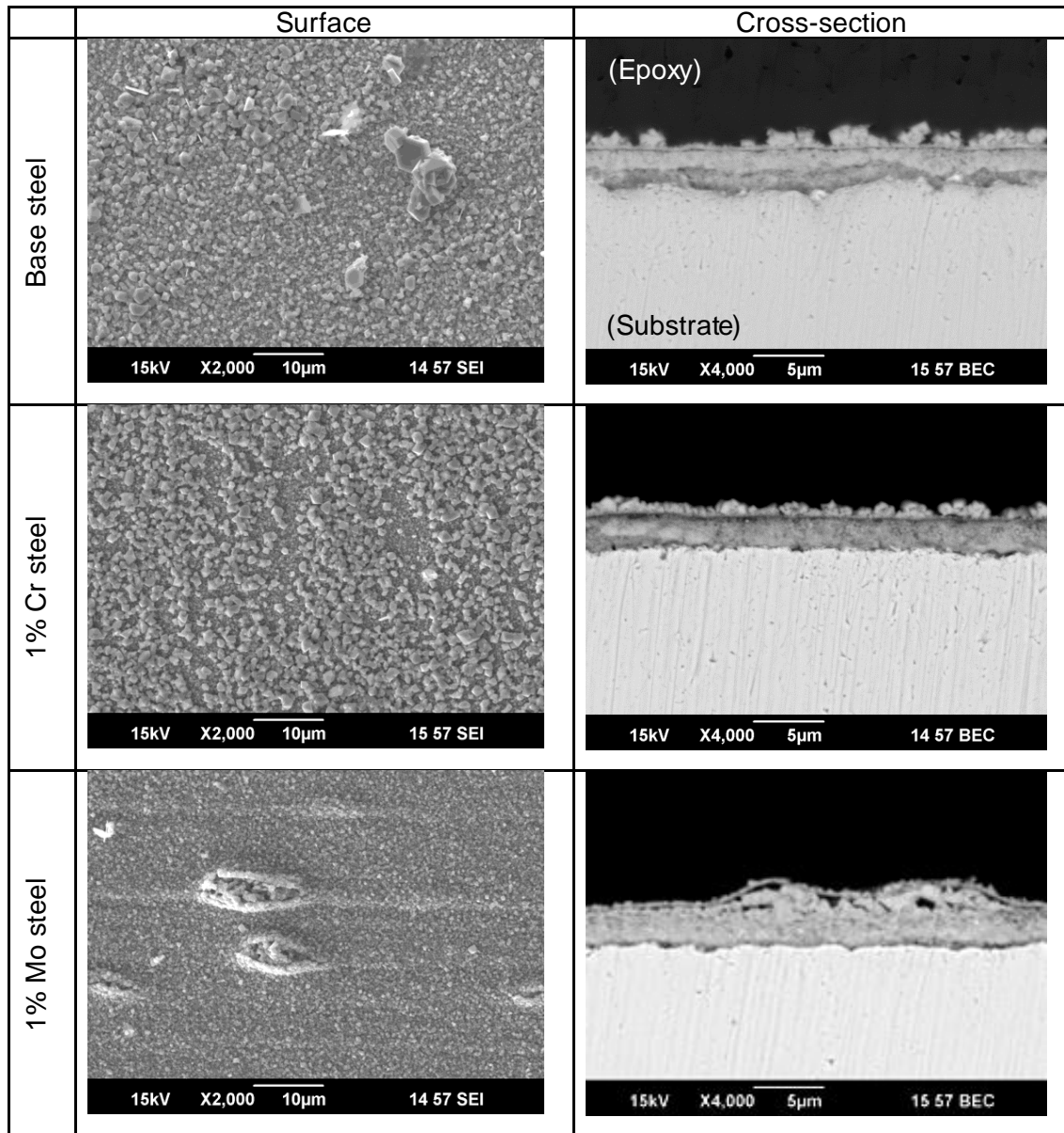


Figure 9: SEM surface and cross-section images of the corroded samples at the end of the exposure at pH 4.2 and 80°C.

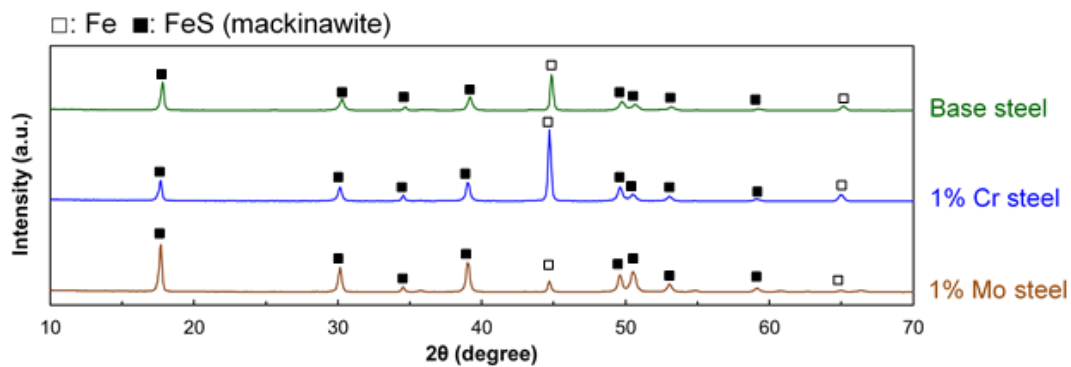


Figure 10: Results of XRD analysis for the corroded samples at the end of the exposure.

DISCUSSION

In the present study (CO₂/ 10% H₂S environments), the presence of 1 wt. % Mo showed no beneficial effect on the corrosion resistance. On the other hand, the presence of 1 wt.% Cr showed a beneficial effect for decreasing the corrosion rate during initial stages of exposure, especially at pH 5.7 condition. In addition, it is likely that the above effects of Mo and Cr on corrosion rate showed the dependency on the testing conditions such as solution pH since the variations of corrosion rates at initial stage of exposure were varied between the results from initial pH 5.7 and initial pH 4.2 in this study. Thus, the probable causes behind the effect of the small amount of Cr and Mo in the CO₂/ 10% H₂S conditions are discussed focusing on the formation mechanism of the corrosion product layers.

Formation mechanism of the corrosion product layers in the CO₂/H₂S environment

The layer of FeS, also known as mackinawite, forms on the steel surface in H₂S environments and confers some protection by slowing down the corrosion process as a result of mass transfer resistance set by the layer, blocking the steel surface and making it unavailable for corrosion. The overall precipitation/dissolution reaction for FeS can be represented by:



And the main driving force for precipitation of FeS is its saturation level defined as follows:

$$S_{\text{FeS(mackinawite)}} = \frac{c_{\text{Fe}^{2+}} \cdot c_{\text{S}^{2-}}}{K_{\text{sp,s}^2}} \quad (4)$$

where, $c_{\text{Fe}^{2+}}$ is the ferrous ion concentration, $c_{\text{S}^{2-}}$ is the bisulfide ion concentration, and $K_{\text{sp,mack}}$ is the solubility limit of FeS (mackinawite). FeS will not form if the saturation level is less than 1.

Figure 11 shows the calculation results of the dependency of the S_{FeS} and S_{FeCO_3} on solution pH and Fe^{2+} concentration at 80°C with 0.48 bar of CO₂ partial pressure and 0.053 bar of H₂S partial pressure. The water chemistry and equilibrium constants that were used for constructing this chart are derived from open literature.²⁹⁻³¹ The $S_{\text{FeS}} = 1$ line represents saturation with respect to FeS while the two dashed lines representing the saturation range between 0.5 and 2 are plotted adjacent to the saturation line. Compared to FeCO₃, FeS (mackinawite) would form at lower Fe^{2+} concentration and lower pH.

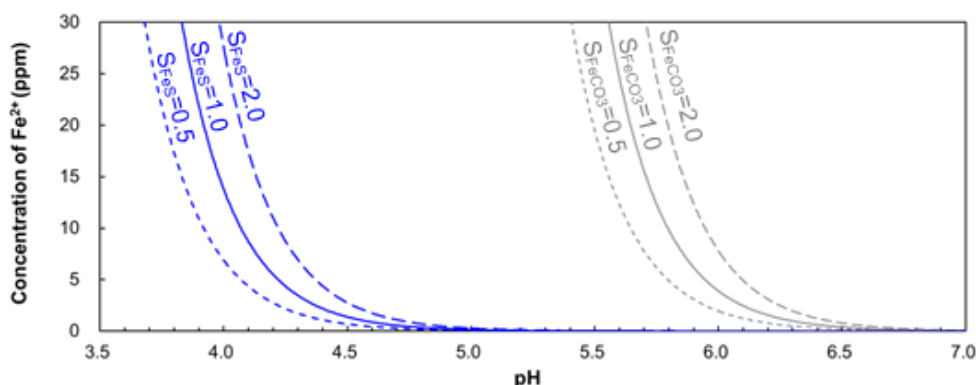


Figure 11: Effect of solution pH and Fe^{2+} concentration on the saturation degree of FeS (S_{FeS}) and FeCO_3 (S_{FeCO_3}) in 1wt.%NaCl at 80°C with $p\text{CO}_2$ of 0.48 bar and $p\text{H}_2\text{S}$ of 0.053 bar.

The measured Fe^{2+} concentrations in the bulk solution with time were shown in Figure 12 for pH 5.7 and pH 4.2 conditions. For both conditions, as corrosion proceeded, the Fe^{2+} was released into the bulk

solution. In the pH 5.7 condition, the concentration of Fe^{2+} in the bulk solution was lower than that in the pH 4.2 condition. However, as shown in Figure 11, the water chemistry in bulk solution could make it easier to reach higher S_{FeS} ($>>1$) in the condition at pH 5.7 than that in the condition at pH 4.2. Although the corrosion behavior at the initial stage of exposure (up to around 20 hours) was different among the three steels, S_{FeS} close to steel surface could reach to high ($>>1$) at a later stage of exposure. Then, eventually the protective FeS layer could form and the corrosion rates of the three steels could reach to low values (Figure 3). In the case of the condition at pH 4.2, based on the comparison of Figure 4 and Figure 8, the concentration of Fe^{2+} close to steel surface could reach high enough ($>>1$) to form FeS layer for the three steels at around 20 hours of exposure. This might lead to a smaller difference at initial stage of exposure.

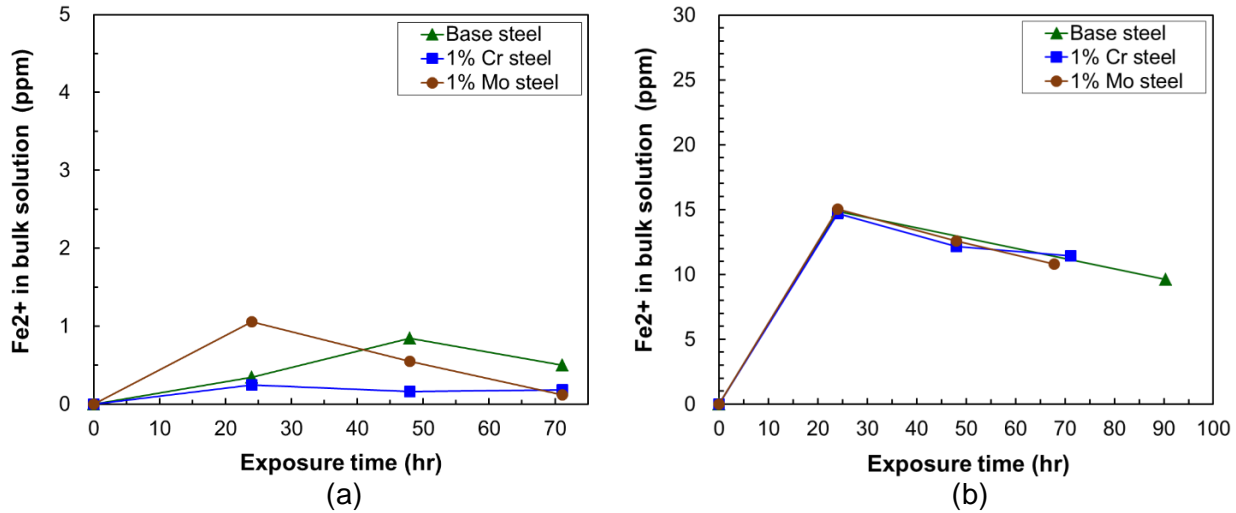


Figure 12: Variations of bulk Fe^{2+} concentrations with time: (a) pH 5.7, 80°C, (b) pH 4.2, 80°C.

Influence of reaction to form the Cr+O compound

During the dissolution of steel substrate, Cr can also dissolve into cationic species such as Cr^{3+} according to Eq. (5). Hydrolysis reactions of cationic species of Cr such could be occurring by Eq. (6) and make it difficult to increase the pH in between the corrosion product layer and the steel surface. According to previous research,^{20,21,32,33} a small amount of Cr alloying could cause the hydrolysis reaction.



The suppression of increasing surface pH by the hydrolysis reaction could lead to generate a higher concentration of Fe^{2+} at the steel surface by promoting corrosion. By this effect, S_{FeS} at the steel surface of the 1% Cr steel could be higher than that of the Base steel in a short time, which could not be detected by the LPR measurement in this study. According to the previous literature,²¹ the condition with a higher saturation value of corrosion product could lead to high nucleation rates. Then, the higher saturation value could lead to the formation of dense layer of corrosion product.³⁴ In the condition at pH 5.7, the higher S_{FeS} at the steel surface by the effect of hydrolysis of Cr could contribute to the formation of protective thin dense layer of FeS at the earlier stage of exposure.

In the case of the condition at pH 4.2, in terms of the variation of corrosion rate with time, the above effect of the formation of hydrolysis of Cr could still remain. However, by reducing the pH from 5.7 to 4.2, as mentioned above, the concentration of Fe^{2+} at the steel surface could increase for all steels.

Then S_{FeS} could reach much higher than 1 and overwhelms the effect of Cr. In addition, according to the Pourbaix diagram of Cr-H₂O system,³⁵ it is likely that the stability of Cr(OH)₃ could be decreased toward the low pH. Thus, the influence of the hydrolysis could be reduced in the condition at pH 4.2 compared to that at pH 5.7.

Influence of reaction to form the Mo+S compound

To discuss the effect of Mo on the formation of FeS layer, the corrosion product formed on the 1% Mo steel after 20 hours of exposure at pH 5.7 and 80°C was further analyzed using FE-EPMA as shown in Figure 13. It shows that a thin layer including Mo and S was observed at the steel surface. According to the previous literature,³⁶ since the solubility of MoS₂ could be much smaller than that of iron sulfide (FeS), MoS₂ could form much faster than FeS. The Mo+S compound observed in Figure 13 might be MoS₂. In this condition, by forming MoS₂, S²⁻ could be consumed rather than by forming FeS. This consumption of S²⁻ by forming MoS₂ could lead to relatively low S_{FeS} at the steel surface compared to that of the Base steel. Therefore, the formation of FeS layer on the steel surface at the initial stage of exposure could be delayed, where the layer was already formed on the surface of the Base steel and the 1% Cr steel. However, 1 wt. % of Mo content in steel was not sufficient to form a protective and continuous layer of MoS₂.

In the case of the condition at pH 4.2 and 80°C, according to the variation of corrosion rate with time, the above effect of Mo on consuming S²⁻ by the formation of MoS₂ may still remain. However, by reducing the pH from 5.7 to 4.2, as mentioned above, the concentration of Fe²⁺ at close to steel surface could increase. Then S_{FeS} could reach to much higher than 1 and overwhelms the effect of Mo.

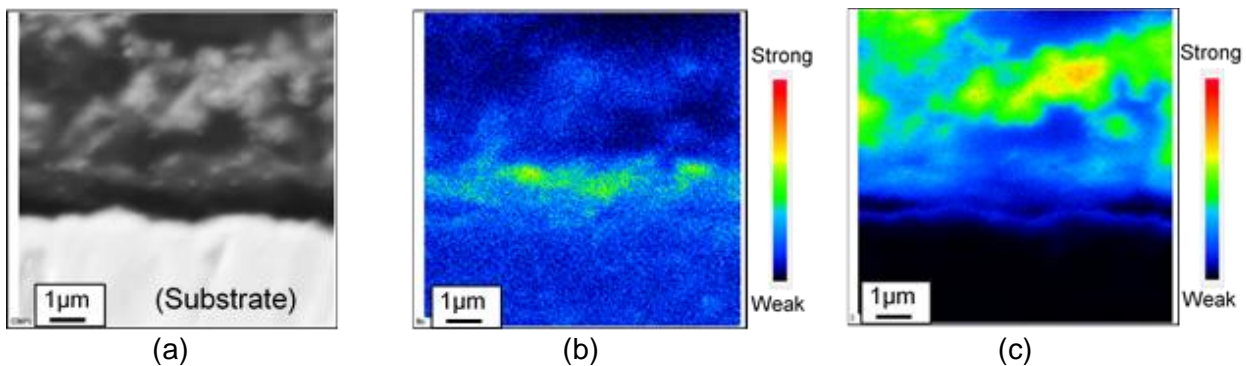


Figure 13: Results of FE-EPMA analysis for corrosion product on the corroded 1%Mo steel after 20 hours of exposure: (a) Backscattered image, (b) Distribution of Mo, (c) Distribution of S.

CONCLUSIONS

The effects of small amounts of Cr and Mo on the corrosion properties of high strength steel in CO₂/H₂S environments were investigated by conducting electrochemical measurement and using surface analytical techniques. The following conclusions are drawn:

- The initial corrosion behavior was different among the Base steel, the 1 wt.% Cr steel and the 1wt.% Mo steel depending on the role of Cr and Mo for the formation of corrosion products.
- The presence of a small amount of Mo delayed the formation of a protective FeS layer due to the formation of MoS₂.
- The presence of a small amount of Cr showed a beneficial effect on the corrosion resistance.
- However, those effects could be varied depending on the pH of testing conditions.

REFERENCES

1. B.J. Orlans-Joliet, F.A. Pellicani, G.C. Gunts, J-J. Servier, Development of C110 Grade for Sour Service, CORROSION/93, paper no. 147 (Houston, TX: NACE 1993),
2. G.P. Echaniz, et al., The Effect of Microstructure on SSC Resistance of Low Alloy Carbon Steels, CORROSION/97, paper no. 50 (Houston, TX: NACE 1993),
3. C.P. Linne, F. Blanchard, F. Puissochet, B.J. Orlans-Joliet, R.S. Hamilton, Heavy Wall Casing in C110 Grade for Sour Service, CORROSION/98, paper no. 117 (Houston, TX: NACE 1998),
4. G. Echaniz, C. Morales, T. Perez, The Effect of Microstructure on the KISSC Low Alloy Carbon Steels, CORROSION/98, paper no. 120 (Houston, TX: NACE 1998),
5. Y. Kuriki, S. Hashizume, Y. Minami, Y. Ishizawa, Development of High Strength SSC-Resistant Low Alloy Steel for OCTG, CORROSION/94, paper no. 74 (Houston, TX: NACE 1994),
6. H. Asahi, K. Nose, Effect of Environmental Conditions on SSC Resistance of C125 OCTG, CORROSION/99, paper no. 601 (Houston, TX: NACE 1999),
7. M. Ueda, et al., Development of 125ksi Grade HSLA Steel OCTG for Mildly Sour Environments, CORROSION/2005, paper no. 05089 (Houston, TX: NACE 2005),
8. J. Leyer, et al., SSC Resistance of a 125 ksi Steel Grade in Slightly Sour Environments, CORROSION/2005, paper no. 05088 (Houston, TX: NACE 2005),
9. A. Di Schino, et al., Metallurgical Design and Development of C125 Grade for Mild Sour Service Application, CORROSION/2006, paper no. 06125 (Houston, TX: NACE 2006),
10. G.M. Waid, R.T. Ault, The Development of a High Strength Casing Steel with Improved Hydrogen Sulfide Cracking Resistance for Sour Oil and Gas Well Applications, CORROSION/79, paper no. 180 (Houston, TX: NACE 1979),
11. P.J. Grobner, D.L. Sponseller, D.E. Diesburg, Effect of Molybdenum Content on the Sulfide Stress Cracking Resistance of AISI 4130-Type Steel with 0.035% Cb, Corrosion 35 (1979) 241.
12. T. Kaneko, et al., Influence of Microstructure on SSC Susceptibility of Low Alloy High Strength Oil Country Tubular Goods, CORROSION/87, paper no. 291 (Houston, TX: NACE 1987),
13. H. Asahi, Y. Sogo, M. Ueno, H. Higashiyama, Metallurgical factors Controlling SSC Resistance of High Strength, Low Alloy Steels, Corrosion 45 (1989) 519.
14. H. Asahi, M. Ueno, Effect of Austenite grain Size of Low Alloy Martensitic Steel on SSC Resistance, CORROSION/90, paper no. 66 (Houston, TX: NACE 1990),
15. H. Asahi, et al., Sulfide Stress Cracking Resistance Evaluation Methods for Steels used in Oil Field Environments-Features and Properties, CORROSION/91, paper no. 29 (Houston, TX: NACE 1991),
16. M.B. Kermani, A. Morshed, Carbon Dioxide Corrosion in Oil and Gas Production-A Compendium, Corrosion 59 (2003) 659-683.
17. L. Wei, X. Pang, K. Gao, Corrosion of Low Alloy Steel and Stainless Steel in Supercritical CO₂/H₂O/H₂S Systems, Corrosion Science 111 (2016) 637-648.
18. P.I. Nice, H. Takabe, M. Ueda, The Development and Implementation of a New Alloyed Steel for Oil and Gas Production Wells, CORROSION/2000, paper no. 00154 (Houston, TX: NACE 2000),
19. H. Takabe, M. Ueda, The Formation Behavior of Corrosion Protective Films of Low Cr Bearing Steels in CO₂ Environments, CORROSION/2001, paper no. 01066 (Houston, TX: NACE 2001),
20. Q. Wu, Z. Zhang, X. Dong, J. Yang, Corrosion Behavior of Low-alloy Steel Containing 1% Chromium in CO₂ Environment, Corrosion Science 75 (2013) 400-408.
21. S. Guo, L. Xu, L. Zhang, W. Chang, M. Lu, Corrosion of Alloy Steels containing 2% Chromium in CO₂ Environments, Corrosion Science 63 (2012) 246-258.
22. B. Ingham, et al., First stages of siderite crystallisation during CO₂ corrosion of steel evaluated using in situ synchrotron small- and wide-angle X-ray scattering, Faraday Discuss. 180 (2015) 171.
23. Y.S. Choi, S. Nescic, H.G. Jung, Effect of Alloying Elements on the Corrosion Behavior of Carbon Steel in CO₂ Environments, Corrosion 74 (2018) 566-576.
24. S.U. Koh, et al., Effect of Molybdenum and Chromium Addition on the Susceptibility to Sulfide Stress Cracking of High-Strength, Low-Alloy Steels, Corrosion 63 (2007) 220-230.
25. E. Wallaert, et al., FeS Corrosion Products Formation and Hydrogen Uptake in a Sour Environment for Quenched & Tempered Steel, Metals 2018,8, 62.

26. Y.Zheng, Electrochemical and Model of H₂S Corrosion of Carbon Steel, Doctor's thesis, Ohio university, 2014
27. M. Stern, A.L. Geary, Electrochemical polarization: I. A theoretical analysis of the shape of polarization curves, *J. Electrochem. Soc.* 104 (1957) 56-63.
28. S.W. Dean, *Handbook on Corrosion Testing and Evaluation*, John Wiley, New York, 1971, p. 171.
29. W. Sun, S. Netic, R.C. Woollam, The Effect of Temperature and Ionic Strength on Iron Carbonate (FeCO₃) Solubility Limit, *Corrosion Science* 51 (2009) 1273-1276.
30. W. Sun, S. Netic, D.Young, R.C. Woollam, Equilibrium Expressions Related to the Solubility of the Sour Corrosion Product Mackinawite, *Ind. Eng. Chem. Res.* **2008**, 47, 1738-1742
31. S. Netic, et al., A Mechanistic Model for Carbon Dioxide Corrosion of Mild Steel in the Presence of Protective Iron Carbonate Films-Part 2: A Numerical Experiment, *Corrosion* 59 (2003) 489-497.
32. W. Li, L. Xu, L. Qiao, J. Li, Effect of Free Cr Content on Corrosion Behavior of 3Cr Steels in a CO₂ Environment, *Applied Surface Science* 425 (2017) 32-45.
33. Z. Liu, et al., Corrosion Behavior of Low-alloy Martensite Steel Exposed to Vapour-saturated CO₂ and CO₂-saturated Brine Conditions, *Electrochimica Acta* 213 (2016) 842-855.
34. M.Gao, et al., The growth mechanism of CO₂ Corrosion Product Films, *Corrosion Science* 53 (2011) 557-568.
35. J.B.Lee, Elevated Temperature Potential-pH Diagrams for the Cr-H₂O, Ti-H₂O, Mo-H₂O and Pt-H₂O Systems, *Corrosion* 37(1981)467-481.
36. M.Ueda and T.Kudo, Effect of Alloying Element on Corrosion Resistance of Ni Base Alloy in Sulfur Containing Sour Environmet, *CORROSION/94*, paper no 69. (Houston, TX: NACE 1993),